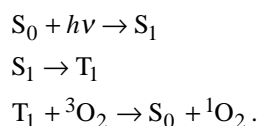

Reverse Intersystem Crossing from a Triplet State of Rose Bengal Populated by Sequential 532-nm plus 1064-nm Laser Excitation

Photodynamic therapy is a treatment in which the combination of a dye, light, and oxygen causes photochemically induced cell death. Observations of this effect occurred at least as early as the end of the last century. In 1900, Raab reported that the dye acridine rapidly killed paramecia when exposed to light, but had no effect in the dark.¹ This observation quickly inspired attempts to use this effect to treat disease. Light and the dye eosin were combined to treat skin cancer in 1903;² however, significant progress in applying photodynamic therapy to the treatment of cancer did not occur until the 1940s and 1950s, when it was discovered that porphyrin-based photosensitive dyes preferentially accumulated in malignant tissues.^{3,4} A sustained series of studies into the mechanisms and applications of photodynamic therapy for the treatment of a broad range of cancers was initiated by Dougherty in the 1970s.⁵ This work led the U.S. Food and Drug Administration in December 1995 to approve the treatment of advanced esophageal cancer using photodynamic therapy with Photofrin[®], a porphyrin-based photosensitizer. In 1998 this approval was extended to cover the treatment of early-stage lung cancer. Other countries have also approved photodynamic therapy for the treatment of bladder, gastric, and cervical cancers. Several review articles have been published that provide an overview of the clinical results as well as the open questions about this therapy that require further research.^{6,7}

The photodynamic effect is a result of three primary processes. First, the ground state of the dye (S_0) is optically excited to produce the excited singlet state (S_1). Population from this excited state is transferred by intersystem crossing (a radiationless transition) to the dye's lowest triplet state (T_1). Finally, collisional energy transfer from the triplet dye to ground-state molecular oxygen (3O_2) produces highly reactive singlet oxygen (1O_2) and returns the dye to its ground state:



The singlet oxygen produced as a result of this three-step process reacts readily with many biological targets and, in sufficient quantity, can destroy a wide variety of cells.

Since the cell damage produced by conventional photodynamic therapy is due to singlet oxygen, an abundant supply of oxygen is critical for an effective treatment. One factor leading to oxygen depletion is the consumption of oxygen by the photodynamic process at a rate faster than it can be resupplied by the circulatory system. In addition, some tumors are inherently poorly oxygenated. A possible solution to this limitation has been suggested by observations that several dyes produce oxygen-independent damage following population of their higher-lying states. It is believed that these states contain sufficient energy to allow for the cleavage of one of the molecular bonds, producing radicals that are even more reactive than singlet oxygen. The production of these radicals does not require the presence of oxygen. Understanding this process requires greater knowledge of the properties of these higher-lying states. In this article we report on our studies of rose bengal, a dye that has been found to produce oxygen-independent damage following excitation of one of its higher-lying triplet states.⁸ In particular, we have studied a decay mechanism based on reverse intersystem crossing from high-lying triplet states that may compete with the bond-cleavage process.

Although intersystem crossing has been identified primarily with transitions from the lowest excited singlet state of a molecule to an even lower-lying triplet state, triplet to singlet intersystem crossing also may occur. Well-known examples of reverse (triplet to singlet) intersystem crossing include E- and P-type delayed fluorescence.⁹ E-type delayed fluorescence, also known as delayed thermal fluorescence, is observed when thermal activation causes population transfer from T_1 back to the more-energetic S_1 state. The strength of E-type delayed fluorescence is temperature dependent, and its lifetime reflects that of T_1 . P-type delayed fluorescence results when the activation energy is provided by triplet-triplet annihilation ($T_1 + T_1 \rightarrow S_1 + S_0$). The strength of the P-type delayed fluorescence increases quadratically with the triplet concentration.

Reverse intersystem crossing may also occur from higher-lying triplet states where intersystem crossing to the singlet manifold competes with direct internal conversion to the lowest triplet state. This process of reverse intersystem crossing from higher-lying triplets is responsible for two-step laser-induced fluorescence (TSLIF) observed in several dyes.^{10–13} The quantum yield of reverse intersystem crossing, Φ_{risc} , can be quite small ($<10^{-5}$),¹⁰ but there are reports of exceptionally high yields ($\Phi_{\text{risc}} > 0.1$) in 9,10-dibromoanthracene,¹¹ several merocyanine derivatives,¹² tetraphenylporphyrin,¹³ erythrosin B,¹³ and rose bengal.¹³

Several reports of reverse intersystem crossing in rose bengal (RB) have been published.^{13–15} Durán and Cilento¹⁴ describe observations of fluorescence following generation of RB triplets by energy transfer from excited triplet acetone. It was believed that higher-lying triplets were populated through triplet-triplet excitation transfer and subsequently relaxed to S_1 through reverse intersystem crossing. The magnitude of the emission was compared for a series of xanthene dyes (fluorescein, eosin, and rose bengal), which revealed that heavy-atom substitution enhanced the effect. This process was not associated with a particular triplet state, and no attempt was made to quantify its yield. Ketsle *et al.*¹⁵ investigated transient absorption changes following two-pulse excitation (532 nm + 694 nm) of various fluorescein derivatives, including rose bengal, incorporated in polymer hosts. Photobleaching of the T_1 absorption due to the second pulse was observed to have a component that was irreversible on the microsecond time scale. It was observed that the decrease in concentration of T_1 equaled the increase in concentration of S_0 , providing evidence for a photophysical rather than photochemical process. Fluorescence emission was also observed coincident with the second pulse. A reverse intersystem crossing quantum yield of 0.72 was reported for T_3 , the triplet state excited by red light. Most recently, the work of Reindl and Penzkofer¹³ reported an 80% quantum yield of reverse intersystem crossing for T_4 , the state excited through absorption of green light by T_1 . Using a model of the population dynamics, the yield was extracted from measurements of the pulse-to-pulse variation in fluorescence for a train of picosecond pulses.

The present work is the first study to identify and investigate the properties of T_2 , a triplet state in rose bengal populated by near-infrared light ($\lambda = 1064$ nm). We have used laser flash photolysis and two-step laser-induced fluorescence measurements to determine the triplet-triplet absorption cross-section spectrum in the near infrared and the quantum yield of reverse intersystem crossing and lifetime of T_2 . In addition,

upper limits on the reverse intersystem crossing yield for T_3 are established.

Experimental

The foundation of the laser system is a mode-locked Nd:YAG laser that generates a train of pulses at 76 MHz. Every 400 ms a single pulse is selected using an electro-optic switch and amplified using a regenerative amplifier followed by a flashlamp-pumped two-pass amplifier (both Nd:YAG). The amplified pulses have a wavelength of 1064 nm, a pulse length of ~ 190 ps, and energies exceeding 2 mJ. The second harmonic is generated from this pulse using a KDP crystal, resulting in a pulse with a wavelength of 532 nm, a pulse length of ~ 134 ps, and an energy greater than 250 μJ .

The experimental setup for the laser flash photolysis measurements is shown in Fig. 77.33 using the symbols defined in Table 77.II. In this configuration the second-harmonic pulse ($\lambda = 532$ nm) is separated from the fundamental by a dichroic mirror (DM) with any residual light at the fundamental wavelength ($\lambda = 1064$ nm) further attenuated by a filter (F). The majority of this frequency-doubled pump pulse is focused by a cylindrical lens (CL) onto the masked sample cuvette, exciting a 2-mm by 1-cm cross-sectional area. A small fraction of the pump pulse is reflected by a glass plate (BS) prior to the cylindrical lens, attenuated by neutral density filters, and then detected by silicon photodiode PD1. This signal is captured by gated integrator GI1 and transferred to a computer. By removing the sample cuvette and placing an energy meter behind the beam mask, the pump pulse monitor signal measured by PD1 can be calibrated with respect to the energy reaching the

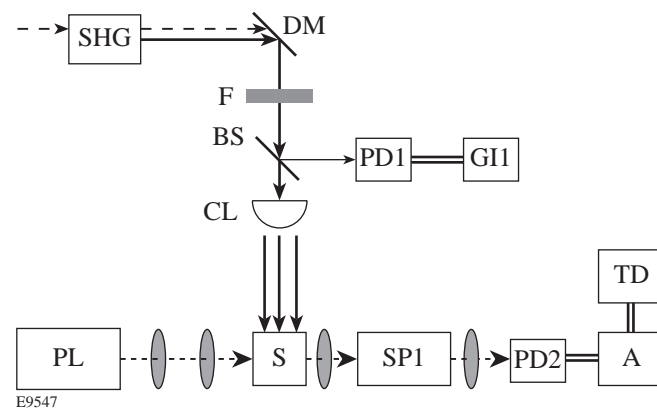


Figure 77.33
Experimental setup for laser flash photolysis measurements. See Table 77.II for symbol definitions.

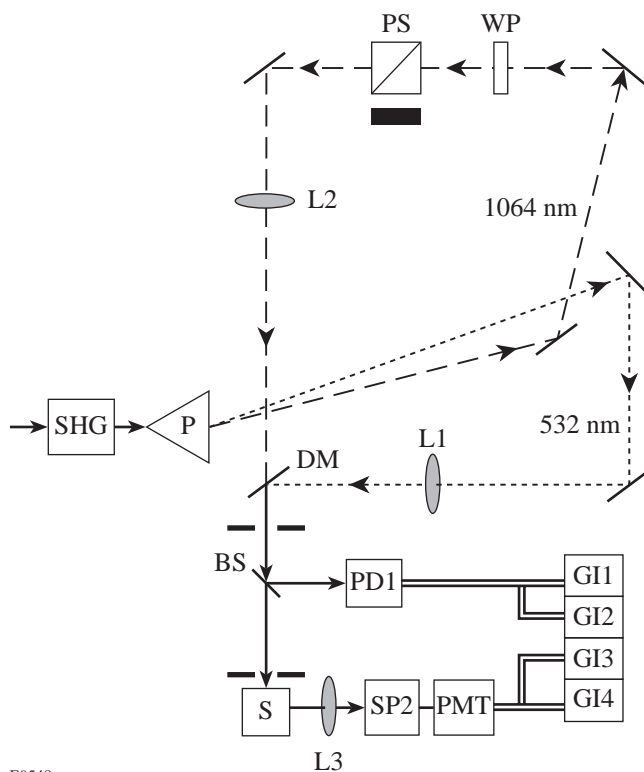
Table 77.II: Equipment used in the laser flash photolysis and two-step laser-induced fluorescence experiments.

	Description	Manufacturer, Model
A	Fast amplifier	EG&G, 574
BS	Glass plate (microscope slide)	
CL	Cylindrical lens	
DM	Dichroic mirror, R@532 nm, T@1064 nm	
F	Short-pass filter	Schott, KG3
GI1-4	Gated integrator	Stanford Research Systems, 250
L1-3	Lenses	
P	Prism	
PD1-2	Silicon photodiodes	EG&G, FND-100
PL	Mercury lamp Fast shutter Long-pass filter	Vincent Associates, Uniblitz VS25 Schott, RG695
PMT	Photomultiplier tube	Burle, 6199
PS	Polarizing beam splitter	
S	Sample cuvette and beam mask	
SHG	Second-harmonic generator (KDP crystal)	
SP1	Monochromator, bandwidth ~13 nm	Instruments SA, H20
SP2	Monochromator, bandwidth ~4 nm	Photon Technology Intl., 102
TD	Digitizing oscilloscope	Hewlett-Packard, HP54201A
WP	Half-wave plate ($\lambda = 1064$ nm)	

sample. Transient absorption changes are probed by a broad-band light beam traveling along the length of the irradiated zone (perpendicular to the pump pulse). The probe pulse has a 20-ms duration and is produced by a mercury lamp followed by a long-pass filter and a fast mechanical shutter. This collection of elements is represented by PL in Fig. 77.33. The probe pulse passes through monochromator SP1 before being detected by silicon photodiode PD2. The photodiode signal is increased by multistage amplifier A and then recorded by digital oscilloscope TD. The average signal from 64 shots at 9-bit resolution is then transferred to a computer for analysis.

The two-step laser-induced fluorescence measurements probing T_2 are made with the optical layout shown in Fig. 77.34. To achieve a high degree of spectral separation between the fundamental and second-harmonic pulses, prism P is used to spatially disperse the two beams. The first pump pulse (P1) has a wavelength of 532 nm, and the second pump pulse (P2) has a wavelength of 1064 nm. P2 is delayed by 34 ns relative to P1 by traversal of a greater optical path length.

The delay path includes a half-wave plate followed by a polarizing beam splitter, allowing for continuous variation of the second pump pulse energy. The pump pulses, P1 and P2, are recombined spatially at dichroic mirror DM. The pulses pass through two pinholes, ensuring collimation, before irradiating a 2-mm-diam spot at the sample cuvette. As in the laser flash photolysis layout, a small fraction of the excitation light is reflected by a glass plate to a silicon photodiode. This signal is split before sampling by two gated integrators, GI1 and GI2, which distinguish between the P1 and P2 signals. The pump-pulse signals are calibrated individually using an energy meter. Emission from the excited sample is collected, spectrally resolved using monochromator SP2, and detected by a photomultiplier tube. The signal from the PMT is split and sampled by the gated integrators GI3 and GI4. The temporal gate of GI3 is centered on the fluorescence excited by P1. The center of the GI4 temporal gate is set to be 34 ns later than the center of the GI3 gate, corresponding to the time delay between the pump pulses. Both gates are 20 ns wide. The values of all four gated integrators are recorded by a computer for each shot.



E9548

Figure 77.34
Experimental setup for two-step laser-induced fluorescence measurements.
See Table 77.II for symbol definitions.

Two-step laser-induced fluorescence measurements probing T_3 are made using a similar setup. In this case P2, the 1064-nm pump pulse, is replaced by a 632-nm-wavelength pump pulse, while the first pump pulse remains at 532 nm. The 632-nm pulse is generated by stimulated Raman scattering of the Nd:YAG second harmonic in an 18-cm ethanol cell, resulting in $60 \mu\text{J}/\text{pulse}$ with a pulse length of approximately 80 ps. The 632-nm light is separated from the 532-nm light by a pair of prisms before P2 enters the delay line. The pulses are spatially recombined at the dichroic mirror DM, and from this point the system is identical to the previously described two-step, laser-induced fluorescence apparatus.

Rose bengal was purchased from Sigma (St. Louis) and used without further purification. All experiments were carried out in phosphate-buffered saline with a pH of 7. Effects of photobleaching were minimized by continuously stirring all samples with a micro-stirbar during irradiation. Photobleaching was monitored by measuring the decrease in fluorescence as a function of the number of excitation pulses. There was a less-than-5% decrease in fluorescence after more than 3700 two-

step excitations. Samples had a concentration of approximately $20 \mu\text{M}$ and were stored in the dark prior to use.

Analysis

Several photophysical parameters associated with an upper triplet state can be determined from two-step laser-induced fluorescence (TSLIF) measurements collected over a range of second pump-pulse (P2) fluences. These measurements are sensitive to the lifetime of the upper triplet state excited by P2, the quantum yield of intersystem crossing from this state back to the singlet manifold, and its thermalization rate. The upper triplet photophysical parameters are determined by fitting a model of the two-step laser-induced fluorescence process to the fluence-dependent TSLIF data.

The kinetic model used to analyze the TSLIF experiments is shown in Fig. 77.35(a). The rate equations describing this model are

$$\begin{aligned} \frac{dp_{S_0}}{dt} &= -\sigma_{S_0S_1}(p_{S_0} - p_{S_1'}) I_1(t) \\ &\quad + (1 - \Phi_{\text{isc}}) \tau_{S_1}^{-1} p_{S_1} + \tau_{T_1}^{-1} p_{T_1}, \\ \frac{dp_{T_1}}{dt} &= \Phi_{\text{isc}} \tau_{S_1}^{-1} p_{S_1} - \tau_{T_1}^{-1} p_{T_1} - \sigma_{T_1T_4} (p_{T_1} - p_{T_4}) I_1(t) \\ &\quad - \sigma_{T_1T_n} (p_{T_1} - p_{T_n}') I_2(t) \\ &\quad + (1 - \Phi_{\text{isc}, T_4}) \tau_{T_4}^{-1} p_{T_4} + (1 - \Phi_{\text{isc}, T_n}) \tau_{T_n}^{-1} p_{T_n}, \\ \frac{dp_{S_1}}{dt} &= k_r p_{S_1'} - \tau_{S_1}^{-1} p_{S_1}, \\ \frac{dp_{S_1'}}{dt} &= \sigma_{S_0S_1} (p_{S_0} - p_{S_1'}) I_1(t) - k_r p_{S_1'} \\ &\quad + \Phi_{\text{isc}, T_4} \tau_{T_4}^{-1} p_{T_4} + \Phi_{\text{isc}, T_n} \tau_{T_n}^{-1} p_{T_n}, \\ \frac{dp_{T_n}}{dt} &= k_{r, T_n} p_{T_n}' - \tau_{T_n}^{-1} p_{T_n}, \\ \frac{dp_{T_n}'}{dt} &= \sigma_{T_1T_n} (p_{T_1} - p_{T_n}') I_2(t) - k_{r, T_n} p_{T_n}', \\ \frac{dp_{T_4}}{dt} &= \sigma_{T_1T_4} (p_{T_1} - p_{T_4}) I_1(t) - \tau_{T_4}^{-1} p_{T_4}, \end{aligned} \quad (1)$$

where the p_i 's are the populations of $S_0, T_1, S_1, S'_1, T_n, T'_n$, and T_4 (arranged in order of increasing energy), where $n = 2$ or 3 . Table 77.III lists the definitions and values of the photophysical parameters. The unknown parameters are Φ_{risc, T_n} , τ_{T_n} , and k_{r, T_n} . The pump pulses P1 and P2 have a Gaussian temporal profile such that

$$I_1(t) = \frac{F_1}{\sqrt{2\pi\delta_1^2}} \exp\left[-(t + \Delta/2)^2 / (2\delta_1^2)\right] \quad (2)$$

and

$$I_2(t) = \frac{F_2}{\sqrt{2\pi\delta_2^2}} \exp\left[-(t - \Delta/2)^2 / (2\delta_2^2)\right], \quad (3)$$

where F_1 and F_2 are the fluences, δ_1 and δ_2 are related to the full-width-at-half-maximum pulse lengths by FWHM

$= \sqrt{8 \ln 2} \delta$, and Δ is the time delay between the peaks of P1 and P2.

Excited-state absorption from states other than T_1 has been neglected. Previous experiments have found no evidence for absorption of 532-nm light by S_1 .¹⁶ The state T_4 may absorb 532-nm light and thus populate an even higher-lying state, but we assume with Reindl and Penzkofer¹³ that any such extremely high-lying state will relax back to T_4 immediately. This process would affect transmission measurements, but since the present studies are concerned only with emission, it appears reasonable to omit it in this case. Finally, absorption by T_n is also not included in this model. The validity of this assumption will be discussed in the **Results** section.

As a result of the large time delay between the pump pulses ($\Delta = 34$ ns), it is possible to separate the system of rate equations [(Eq. (1))] into two subsets. The set of equations describing the effects of the first pump pulse is

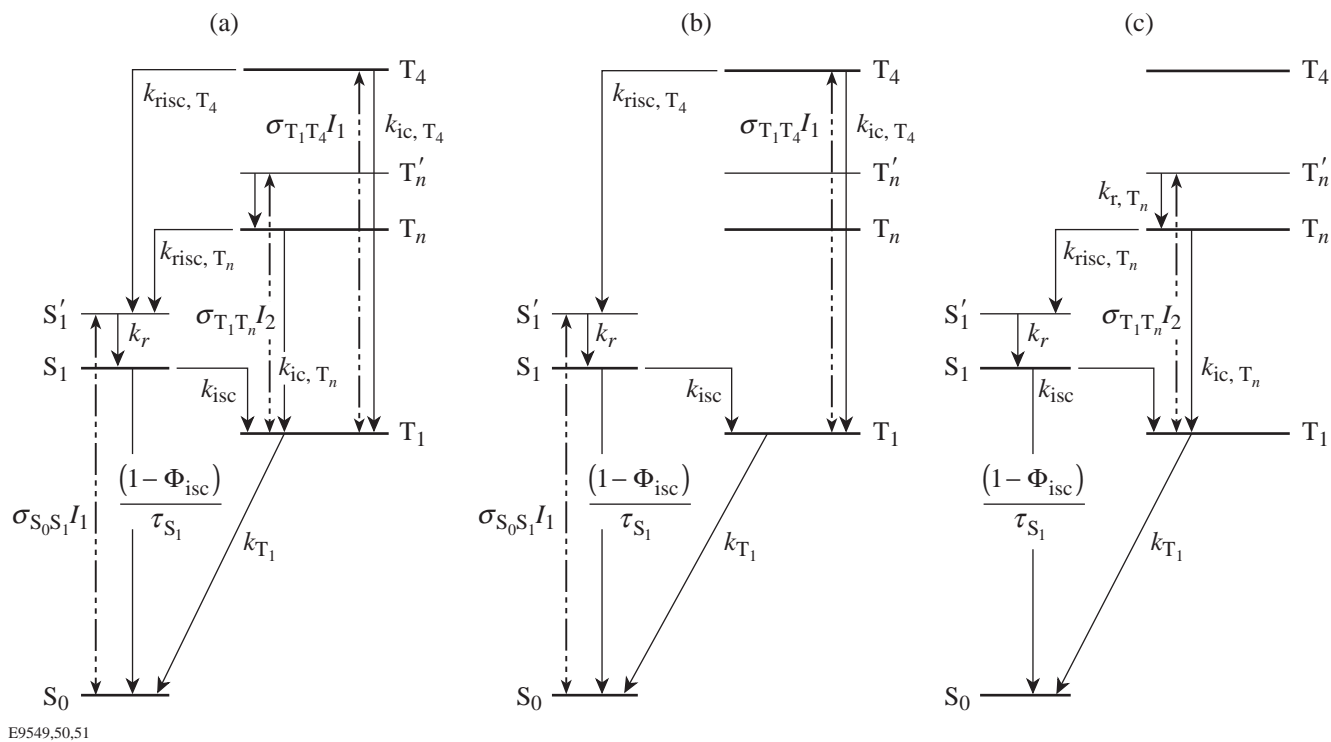


Figure 77.35

Energy-level scheme for description of two-color excitation dynamics. (a) Complete two-step model, (b) P1 subset of model, (c) P2 subset of model. See Table 77.III for parameter descriptions and values.

Table 77.III: Parameters used in the two-step laser-induced fluorescence model for rose bengal.

Parameter	Description	Value	Reference
$\sigma_{S_0S_1}$	Ground-state absorption cross section at 532 nm ($S_0 + \hbar\omega \rightarrow S'_1$)	$1.8 \times 10^{-16} \text{ cm}^2$	16
$\sigma_{T_1T_2}$	Triplet absorption cross section ($T_1 + \hbar\omega \rightarrow T'_2$)	$(1.1 \pm 0.1) \times 10^{-16} \text{ cm}^2$	This work
$\sigma_{T_1T_4}$	Triplet absorption cross section at 532 nm ($T_1 + \hbar\omega \rightarrow T_4$)	$7.4 \times 10^{-17} \text{ cm}^2$	16
τ_{S_1}	S_1 lifetime	89 ps	16–18
τ_{T_1}	Lifetime of T_1 (includes both phosphorescence and oxygen quenching)	3 μs	19
τ_{T_4}	Lifetime of T_4	50 fs	16
τ_{T_n}	Lifetime of T_n	fitting parameter	
Φ_{isc}	Intersystem crossing yield ($S_1 \rightarrow T_1$)	0.98	18,19
Φ_{risc,T_4}	Reverse intersystem crossing yield ($T_4 \rightarrow S'_1$)	0.8	13
Φ_{risc,T_n}	Reverse intersystem crossing yield ($T_n \rightarrow S'_1$)	fitting parameter	
F_1	First pump-pulse fluence ($\lambda = 532 \text{ nm}$)	$(8.8 \pm 0.5) \times 10^{15} \text{ photons/cm}^2$	
F_2	Second pump-pulse fluence ($\lambda = 1064 \text{ nm}$)	varied	
k_{ic,T_4}	Internal conversion rate ($T_4 \rightarrow T_1$)	$(1 - \Phi_{\text{risc},T_4}) / \tau_{T_4}$	
k_{ic,T_n}	Internal conversion rate ($T_n \rightarrow T_1$)	$(1 - \Phi_{\text{risc},T_n}) / \tau_{T_n}$	
k_{isc}	Intersystem crossing rate	$\Phi_{\text{isc}} / \tau_{S_1}$	
k_{r,T_n}	Thermalization rate ($T'_n \rightarrow T_n$)	fitting parameter	
k_r	Thermalization rate ($S'_1 \rightarrow S_1$)	10^{12} s^{-1}	16
k_{risc,T_4}	Reverse intersystem crossing rate ($T_4 \rightarrow S'_1$)	$\Phi_{\text{risc},T_4} / \tau_{T_4}$	
k_{risc,T_n}	Reverse intersystem crossing rate ($T_n \rightarrow S'_1$)	$\Phi_{\text{risc},T_n} / \tau_{T_n}$	
k_{T_1}	T_1 relaxation rate	$1 / \tau_{T_1}$	

$$\begin{aligned}
 \frac{dp_{S_0}}{dt} &= -\sigma_{S_0S_1}(p_{S_0}-p_{S_1'})I_1(t) + (1-\Phi_{isc})\tau_{S_1}^{-1}p_{S_1} \\
 &\quad + \tau_{T_1}^{-1}p_{T_1}, \\
 \frac{dp_{T_1}}{dt} &= \Phi_{isc}\tau_{S_1}^{-1}p_{S_1} - \tau_{T_1}^{-1}p_{T_1} - \sigma_{T_1T_4}(p_{T_1}-p_{T_4})I_1(t) \\
 &\quad + (1-\Phi_{risc,T_4})\tau_{T_4}^{-1}p_{T_4}, \\
 \frac{dp_{S_1}}{dt} &= k_r p_{S_1'} - \tau_{S_1}^{-1}p_{S_1}, \\
 \frac{dp_{S_1'}}{dt} &= \sigma_{S_0S_1}(p_{S_0}-p_{S_1'})I_1(t) - k_r p_{S_1'} \\
 &\quad + \Phi_{risc,T_4}\tau_{T_4}^{-1}p_{T_4}, \\
 \frac{dp_{T_4}}{dt} &= \sigma_{T_1T_4}(p_{T_1}-p_{T_4})I_1(t) - \tau_{T_4}^{-1}p_{T_4},
 \end{aligned} \tag{4}$$

which are used for $t = -\infty$ to $t = 0$. The time $t = 0$ is midway between the peaks of P1 and P2, which are separated by a delay much greater than their pulse lengths and the lifetimes of all excited states except T_1 . The processes included in this first segment, where only the effects of P1 are relevant, are shown in Fig. 77.35(b). This set of equations describing the effects of P1 neglects all terms containing I_2 . Since T_n and T_n' are only populated by P2, corresponding terms can be eliminated from Eq. (1) since $p_{T_n} = p_{T_n'} = 0$. The process of reverse intersystem crossing is included in this model of the interaction of P1 with the sample. The first pump pulse may be absorbed by both S_0 and by any T_1 population created by preceding parts of the same pulse. Absorption of P1 light by the T_1 state populates the T_4 state, which has been shown to have a high yield of reverse intersystem crossing.¹³ It is necessary to include this process for pulses longer than the $S_1 \rightarrow T_1$ intersystem crossing time since it can lead to an apparent enhancement of the fluorescence yield, particularly at fluences resulting in depletion of the ground state. At the P1 fluence used experimentally, the solution of Eq. (4), which includes the reverse intersystem crossing process, led to a 29%-greater integrated fluorescence compared to an otherwise identical set of equations that neglected this process. It is important to emphasize that the reverse intersystem crossing described above occurs from the triplet state populated by secondary absorption of the first pump pulse and is easily distinguished temporally from the process this experiment is designed to measure: reverse inter-

system crossing from the triplet state populated by the second pump pulse.

The effects of P1 and P2 can be separated cleanly since the system has relaxed such that only S_0 and T_1 are populated at $t = 0$. The effects of only the second pump pulse are considered from this time to $t = +\infty$. The model of this second excitation step is shown in Fig. 77.35(c). The equations describing this segment are

$$\begin{aligned}
 \frac{dp_{S_0}}{dt} &= (1-\Phi_{isc})\tau_{S_1}^{-1}p_{S_1} + \tau_{T_1}^{-1}p_{T_1}, \\
 \frac{dp_{T_1}}{dt} &= \Phi_{isc}\tau_{S_1}^{-1}p_{S_1} - \tau_{T_1}^{-1}p_{T_1} - \sigma_{T_1T_n}(p_{T_1}-p_{T_n'})I_2(t) \\
 &\quad + (1-\Phi_{risc,T_n})\tau_{T_n}^{-1}p_{T_n}, \\
 \frac{dp_{S_1}}{dt} &= k_r p_{S_1'} - \tau_{S_1}^{-1}p_{S_1}, \\
 \frac{dp_{S_1'}}{dt} &= -k_r p_{S_1'} + \Phi_{risc,T_n}\tau_{T_n}^{-1}p_{T_n}, \\
 \frac{dp_{T_n}}{dt} &= k_{r,T_n} p_{T_n'} - \tau_{T_n}^{-1}p_{T_n}, \\
 \frac{dp_{T_n'}}{dt} &= \sigma_{T_1T_n}(p_{T_1}-p_{T_n'})I_2(t) - k_{r,T_n} p_{T_n'}.
 \end{aligned} \tag{5}$$

In this segment all terms containing I_1 and p_{T_4} , the population of T_4 , are dropped from Eq. (1).

The fluorescence due to the two pulses is proportional to the population of S_1 such that

$$f_1 = \frac{\Phi_f}{\tau_{S_1}} \int_{-\infty}^0 p_{S_1}(t) dt \tag{6}$$

and

$$f_2 = \frac{\Phi_f}{\tau_{S_1}} \int_0^{+\infty} p_{S_1}(t) dt, \tag{7}$$

where Φ_f is the fluorescence yield. The two-step, laser-induced fluorescence ratio f_R is defined by

$$f_R \equiv \frac{f_2}{f_1}. \quad (8)$$

This is a convenient quantity to compare with experimental results since fluorescence yield, collection, and detection efficiency factors are eliminated.

The T_n photophysical parameters are determined by fitting this model of the two-step, laser-induced fluorescence process to the fluence-dependent f_R obtained experimentally. As will be discussed later, extraction of the parameters requires f_R measurements over a range of P2 fluences, which, at the upper limit, are sufficient to partially deplete the lowest triplet state. In addition, the length of the second pump pulse must exceed the lifetime of T_n . A numerical approach is required since under these conditions analytical solutions cannot be obtained easily. The numerical analysis consists of three major components: (a) a calculation of the fluence-dependent f_R for a given set of T_n photophysical parameters, (b) an algorithm that optimizes these parameters to provide the best fit to the experimental data, and (c) an estimate of the precision to which the extracted parameters are known based on a randomization and re-optimization technique.

Calculation of the fluence-dependent, two-step laser-induced fluorescence ratio was based on the sequential solution of the rate equations given in Eqs. (4) and (5). These rate equations were solved using Runge–Kutta numerical integration. The agreement between the f_R obtained from this model and the experimental data can be quantified by the χ^2 statistic, which is summed over the set F_1, F_2 for which experimental measurements of the TSLIF ratio, $f_{R,\text{expt}}$, were made. The standard deviations of those measurements are given by $\sigma_{R,\text{expt}}$. The next step is to search parameter space in order to find the values of k_{r,T_n} , τ_{T_n} , and Φ_{risc,T_n} that minimize χ^2 . The optimization algorithm used is the downhill simplex method.²⁰

The downhill simplex method will find the set of parameters that minimizes χ^2 , but it does not report the precision with which these parameters are known given the uncertainties in the experimental measurements. This precision was estimated by running the optimization routine on sets of TSLIF ratio measurements, $f_{R,\text{mix}}$, calculated from

$$f_{R,\text{mix}}(F_1, F_2) = f_{R,\text{expt}}(F_1, F_2) + r\sigma_{R,\text{expt}}(F_1, F_2), \quad (9)$$

where r is a uniformly distributed random number between -1 and 1 . The standard deviations of the parameters found in minimizing ten such data sets provide the estimated precision to which the parameters are known.

An analytical model of two-step laser-induced fluorescence that is limited to low-intensity and low-fluence conditions can be developed. In this regime the fluorescence signals are given by

$$f_1 = a\sigma_{S_0S_1}F_1 \quad (10)$$

and

$$f_2 = a\Phi_{\text{isc}}\Phi_{\text{risc},T_n}\sigma_{S_0S_1}F_1\sigma_{T_1T_n}F_2, \quad (11)$$

where a includes fluorescence yield, collection, and detection factors. Calculating the two-step laser-induced fluorescence ratio from Eqs. (10) and (11) gives

$$f_R = \Phi_{\text{isc}}\Phi_{\text{risc},T_n}\sigma_{T_1T_n}F_2. \quad (12)$$

Although this expression cannot be used to determine τ_{T_n} and k_{r,T_n} , it is useful for estimating upper limits on Φ_{risc,T_n} when there is an undetectable two-step laser-induced fluorescence signal.

Results

The triplet-triplet absorption spectrum of rose bengal in the near infrared (Fig. 77.36) is derived from a series of transient absorption measurements acquired by laser flash photolysis. There is no measurable ground-state absorption in this region. Detector insensitivity prevented the extension of this spectrum beyond 1100 nm. Using the intensity variation method²¹ it was found that the absorption has a peak between 1050 and 1075 nm with a cross section $\sigma_{T_1T_2} = (1.1 \pm 0.1) \times 10^{-16}$ cm².

Figure 77.37 shows two-step laser-induced fluorescence results for T_2 . The ratio of two-step to one-step fluorescence $f_{R,\text{expt}}$ versus the fluence of the second pump pulse ($\lambda_2 = 1064$ nm) is plotted. The first pump-pulse fluence ($\lambda_1 = 532$ nm) was held approximately constant at 3.3 ± 0.2 mJ/cm², and the resulting one-step fluorescence varied by less than 2%. No emission following P2 was detected when P1 was blocked. Each point in this plot represents the average of from 26 to 370 double-pulse excitations. The error bars indicate the corresponding standard deviations. In addition, the spectrum of the 532-nm + 1064-nm excited emission was measured and found to be the same as the $S_1 \rightarrow S_0$ fluorescence spectrum,

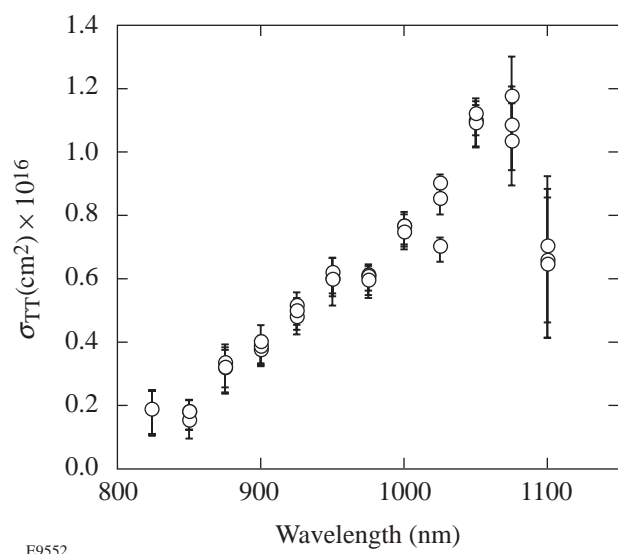


Figure 77.36
Triplet-triplet absorption spectrum of rose bengal in the near infrared.

confirming that the TSLIF results from repopulation of S_1 . The parameters Φ_{risc,T_2} , τ_{T_2} , and k_{r,T_2} can be determined by analyzing the nonlinear dependence of f_R on F_2 using the multistate kinetic model described in the **Analysis** section. This analysis of the data shown in Fig. 77.37 gives $\Phi_{\text{risc},T_2} = 0.0142 \pm 0.0003$, $\tau_{T_2} = 5.8 \pm 1.6$ ps, and $k_{r,T_2} = 1.30 \pm 0.18$ ps $^{-1}$ with $\chi^2 = 0.011$.

Similar measurements probing T_3 ($\lambda_1 = 532$ nm, $\lambda_2 = 632$ nm) failed to detect any two-step laser-induced fluorescence. Based on the fluorescence detection limits, the quantum yield of reverse intersystem crossing from T_3 can be constrained to $\Phi_{\text{risc},T_3} < 0.06$ using Eq. (12) with $\sigma_{T_1T_3}$ determined from Ref. 22 and f_R set equal to the uncertainty in the TSLIF measurement.

Discussion

Although no analytical expression can be given for $f_R(F_1, F_2)$ that is applicable for the high fluences used in these experiments, it is possible to explain qualitatively the shape of the f_R versus F_2 curve shown in Fig. 77.37. This explanation also provides some justification for why the kinetic model analysis is sensitive to the lifetime and thermalization rate of the upper triplet state. Under low-fluence and low-intensity conditions, Eq. (12) predicts that f_R will increase linearly with F_2 . Deviations from the predicted linear response are expected to occur for P2 with sufficiently high intensity or fluence. Under conditions where the pulse length is shorter than the lifetime of T_2 , the saturation fluence $F_{\text{sat}} = (\sigma_{T_1T_2})^{-1}$ for

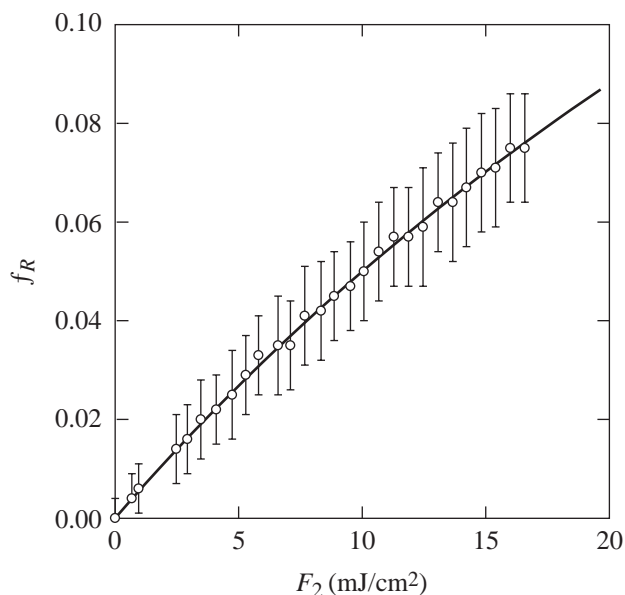


Figure 77.37
Fluence dependence of two-step laser-induced fluorescence ratio f_R . Delay between excitation pulses: 34 ns. Circles are averages of from 26 to 370 double-pulse excitations with error bars indicating the standard deviations. The curve represents the best fit ($\chi^2 = 0.011$) calculated from solutions of Eqs. (4) and (5) using the parameter values given in Table 77.III. The photophysical parameters determined from the fitting procedure are $\Phi_{\text{risc},T_2} = 0.0142 \pm 0.0003$, $\tau_{T_2} = 5.8 \pm 1.6$ ps, and $k_{r,T_2} = 1.30 \pm 0.18$ ps $^{-1}$.

$T_1 \rightarrow T_2$ excitation is 9×10^{15} photons/cm 2 (1.7 mJ/cm 2). Multiple excitations are possible, however, for pulses that are longer than the lifetime of T_2 . This allows the two-step laser-induced fluorescence ratio to continue to grow beyond the short-pulse saturation fluence limit. Limits on the growth of the two-step laser-induced fluorescence are not solely fluence dependent. The maximum rate at which population can be excited to the upper triplet state is limited by the thermalization rate k_{r,T_2} . In addition, the maximum number of excitation cycles that can be achieved during a pulse is limited by the upper triplet lifetime τ_{T_2} and the length of the second pump pulse δ_2 . Since the nonlinear portion of the f_R curve is dependent on the upper triplet lifetime and its thermalization rate, it is possible to extract these parameters from a fit of the kinetic model to data obtained under high-intensity and high-fluence conditions where the deviation from linearity becomes significant.

The multistate kinetic model described in Eq. (1) and Fig. 77.35 is not the only possible explanation for fluorescence following 532-nm + 1064-nm excitation. An alternative

model that deserves consideration includes absorption of 1064-nm light by T_2 to populate T_4 , a state already known to have a high reverse intersystem crossing yield.¹³ On the basis of energetic considerations, the $T_2 \rightarrow T_4$ absorption process appears to be plausible, although restrictions such as those based on parity may disallow this transition. If reverse intersystem crossing were to occur predominantly from T_4 , then the expression for f_R given in Eq. (12) should be modified to give

$$f_R = \Phi_{isc} \Phi_{isc, T_4} \sigma_{T_1 T_2} \sigma_{T_2 T_4} F_2^2. \quad (13)$$

According to this model, f_R increases quadratically rather than linearly in F_2 since population of T_4 from T_1 requires the sequential absorption of two 1064-nm photons. In addition, f_R is expected to saturate at a value greater than $\Phi_{isc} \Phi_{isc, T_4} = 0.78$. The experimental data shown in Fig. 77.37 do not exhibit this behavior, which justifies our elimination of this alternative model.

No two-step laser-induced fluorescence was detected in the 532-nm + 632-nm experiment. This experiment was performed under conditions much less favorable than for the 532-nm + 1064-nm experiment. Both the maximum P2 fluence and the triplet-triplet absorption cross section were significantly less at 632 nm compared to 1064 nm. Even with these limitations, however, the value of Φ_{isc, T_3} can be determined to be less than 0.06. This result disagrees with a yield of 0.72 for this state reported previously.¹⁵

Ketsle *et al.* attempted to measure the yield of reverse intersystem crossing through measurements of the change in T_1 absorption (and therefore, concentration) in a two-step excitation experiment.¹⁵ Immediately following P2, a decrease in the concentration ΔC_{ab} of T_1 was observed, which was followed by a partial recovery ΔC_{ac} , as shown in Fig. 77.38, which is a sketch showing the key features in the transient signal plotted in Fig. I of Ref. 15. The points a , b , and c in Fig. 77.38 represent the times immediately prior to P2, immediately following P2, and after the fast recovery of the transient bleaching, respectively. The lack of complete recovery is due to reverse intersystem crossing from the higher-lying triplet populated by P2. From these concentration changes Ketsle *et al.* calculated the reverse intersystem crossing yield using the formula

$$\frac{\Delta C_{ac}}{\Delta C_{ab}} = \Phi_{isc, T_3}. \quad (14)$$

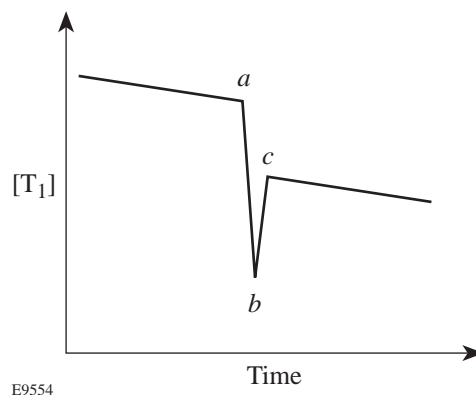


Figure 77.38

Schematic of transient changes in T_1 concentration (based on Fig. I in Ref. 15). The points a , b , and c in the figure represent the times immediately prior to P2, immediately following P2, and after the fast recovery of the transient bleaching, respectively.

Equation (14) attributes the bleaching to the entire fraction undergoing reverse intersystem crossing. It is more appropriate, however, to interpret bleaching as due to the fraction that undergoes reverse intersystem crossing and in addition does not repopulate the triplet manifold through $S_1 \rightarrow T_1$ transfer, implying

$$\frac{\Delta C_{ac}}{\Delta C_{ab}} = \Phi_{isc, T_3} (1 - \Phi_{isc}). \quad (15)$$

Indeed, this latter interpretation of the bleaching fraction agrees with that used by Redmond *et al.*¹² Recalculating a yield based on Eq. (15) using the Ketsle *et al.* bleaching fraction data found in Table I of Ref. 15 gives $\Phi_{isc, T_3} \gg 1$. Since this quantum yield cannot exceed unity, it appears that their experimental data was obtained under conditions in which the assumptions used to derive these equations do not apply. In particular, these equations are valid only under conditions in which ΔC_{ab} is proportional to the number of photons absorbed by T_1 . This can occur only when the length of the exciting pulse is shorter than the lifetime of the upper triplet state ($\delta_2 \ll \tau_{T_3}$) and when the transient absorption detection system is capable of responding on this same time scale. Ketsle *et al.* do not report the length of their second pump pulse but state only that it is from a ruby laser. It appears likely that their excitation pulse is longer than several nanoseconds, which is much greater than the expected upper triplet lifetime of picoseconds or less. In addition, the time response of their transient absorption detection system is not reported. The use of long pulses or slow detection systems with this transient

absorption technique will lead to an underestimate of the number of absorbed photons, thus leading to values of Φ_{risc,T_3} that exceed unity. The equipment requirements are not as demanding for fluorescence methods of measuring reverse intersystem crossing.

Reverse intersystem crossing yields have been calculated for a growing number of molecules. An aspect of this study that makes it of particular interest is that these yields have now been measured for several triplet states of rose bengal. Previous workers in this field have suggested that population excited to T_n relaxes rapidly to the next-lowest triplet state, and that the triplet-singlet transfer is predominantly due to reverse intersystem crossing from this less-energetic state.^{13,23} According to this model, the reverse intersystem crossing yield should be independent of the high-lying triplet state initially excited; experimental measurements clearly contradict this prediction with high yields of $\Phi_{\text{risc},T_4} = 0.80$ if T_4 is initially excited,¹³ to much lower yields of $\Phi_{\text{risc},T_2} = 0.0142$ for the case of direct population of T_2 (measured in this work).

To understand these results it is instructive to consider the energies of the relevant triplet and singlet states. The energies of the singlet states can be estimated from the peaks of the ground-state absorption spectrum. Similarly, the energies of the triplet states relative to T_1 can be estimated from triplet-triplet absorption spectra (the present work and Refs. 8 and 24). The energy of T_1 in methanol is 1.75 eV.²⁵ These results have been compiled in Table 77.IV. The energy gaps between the excited triplet states and the nearest less-energetic singlet state are $\Delta E (T_2-S_2) = 0.51$ eV, $\Delta E (T_3-S_3) = 0.35$ eV, and $\Delta E (T_4-S_4) = 0.08$ eV. Thus we find that the transition with the smallest energy gap exhibits the greatest reverse intersystem crossing yield ($\Phi_{\text{risc},T_2} = 0.0142$, $\Phi_{\text{risc},T_3} < 0.06$, $\Phi_{\text{risc},T_4} = 0.80$). Although this ordering is consistent with a simple interpretation of the energy gap law for nonradiative transitions, which states that reverse intersystem crossing is likely to be most favorable when there is a small energy gap between the triplet state and a nearby singlet, such an interpretation must be considered critically. As developed by Englman and Jortner,²⁶ the energy gap law applies to a particular triplet-singlet pair, whereas here we are considering three such pairs. The strength of the spin-orbit coupling between different states may vary by several orders of magnitude. Since we do not know the values of the coupling parameters for the three transitions under consideration, it is impossible to definitively attribute the entire variation in reverse intersystem crossing yield to differences in the energy gap.

Table 77.IV: Energies of rose bengal excited states. Singlet-state energies are estimated from the ground-state absorption spectrum. Triplet-state energies are estimated from the T_1 absorption spectrum.

State	Energy (eV)	Ref.
S_1	2.10	This work
S_2	2.41	This work
S_3	3.51	This work
S_4	3.95	This work
T_1	1.75	25
T_2	2.92	This work
T_3	3.86	8
T_4	4.03	24

Conclusion

We have presented what we believe to be the first study of a triplet state of rose bengal that is produced by 1064-nm excitation of T_1 . The triplet-triplet absorption cross section was measured between 825 nm and 1100 nm. This state was further characterized using two-step laser-induced fluorescence to determine its thermalization rate, lifetime, and quantum yield of reverse intersystem crossing. Similar two-step laser-induced fluorescence measurements were made of the triplet excited by 632-nm light.

In earlier work, the reverse intersystem crossing yield was predicted to be independent of which higher-lying triplet state was initially excited. The present work finds that the yields for triplets excited by red and near-infrared light, T_3 and T_2 , are much less than those reported earlier for the more-energetic state T_4 , which is populated by green light.¹³ An analysis of the triplet-triplet absorption spectrum and the ground-state absorption spectrum shows that T_4 is energetically close to a state in the singlet manifold, whereas the corresponding gaps are significantly greater for T_2 and T_3 .

ACKNOWLEDGMENT

This work has been supported by the U.S. Department of Energy Office of Inertial Confinement Fusion under Cooperative Agreement No. DE-FC03-92SF19460, the University of Rochester, the New York State Energy Research and Development Authority, and by U.S. Public Health Service grant CA68409. The support of DOE does not constitute an endorsement by DOE of the views expressed in this article.

REFERENCES

1. O. Raab, *Infusoria Z. Biol.* **39**, 524 (1900).
2. V. H. Tappeiner and A. Jesionek, *Muench. Med. Wochenshr.* **47**, 2042 (1903).
3. F. H. J. Figge, G. S. Weiland, and L. O. J. Manganiello, *Proc. Soc. Exp. Biol. Med.* **68**, 640 (1948).
4. R. L. Lipson, E. J. Baldes, and A. M. Olsen, *J. Natl. Cancer Inst.* **26**, 1 (1961).
5. T. J. Dougherty, *J. Natl. Cancer Inst.* **52**, 1333 (1974).
6. H. I. Pass, *J. Natl. Cancer Inst.* **85**, 443 (1993).
7. T. J. Dougherty *et al.*, *J. Natl. Cancer Inst.* **90**, 889 (1998).
8. G. Smith *et al.*, *Photochem. Photobiol.* **59**, 135 (1994).
9. S. P. McGlynn, T. Azumi, and M. Kinoshita, *Molecular Spectroscopy of the Triplet State* (Prentice-Hall, Englewood Cliffs, NJ, 1969).
10. S. Kobayashi, K. Kikuchi, and H. Kokubun, *Chem. Phys. Lett.* **42**, 494 (1976); S. Kobayashi, K. Kikuchi, and H. Kokubun, *Chem. Phys.* **27**, 399 (1978).
11. W. G. McGimpsey and J. C. Scaiano, *J. Am. Chem. Soc.* **111**, 335 (1989).
12. R. W. Redmond *et al.*, *J. Phys. Chem. A* **101**, 2773 (1997).
13. S. Reindl and A. Penzkofer, *Chem. Phys.* **211**, 431 (1996).
14. N. Durán and G. Cilento, *Photochem. Photobiol.* **32**, 113 (1980).
15. G. A. Ketsle, L. V. Levshin, and S. N. Letuta, *Opt. Spectrosc. (USSR)* **68**, 202 (1990).
16. H. Stiel *et al.*, *J. Photochem. Photobiol. B: Biol.* **33**, 245 (1996).
17. G. R. Fleming *et al.*, *J. Am. Chem. Soc.* **99**, 4306 (1977).
18. M. A. J. Rodgers, *Chem. Phys. Lett.* **78**, 509 (1981).
19. P. C. C. Lee and M. A. J. Rodgers, *Photochem. Photobiol.* **45**, 79 (1987).
20. W. H. Press *et al.*, *Numerical Recipes in FORTRAN: The Art of Scientific Computing*, 2nd ed. (Cambridge University Press, Cambridge, England, 1992).
21. I. Carmichael and G. L. Hug, *J. Phys. Chem. Ref. Data* **15**, 1 (1986).
22. P. Murasecco-Suardi *et al.*, *Helv. Chim. Acta.* **70**, 1760 (1987).
23. H. Fukumura *et al.*, *J. Photochem. Photobiol. A: Chem.* **42**, 283 (1988).
24. C. R. Lambert *et al.*, *Photochem. Photobiol.* **63**, 154 (1996).
25. T. Shen *et al.*, *J. Photochem. Photobiol. A: Chem.* **47**, 203 (1989).
26. R. Englman and J. Jortner, *Mol. Phys.* **18**, 145 (1970).